

Radial velocity photon limits for the dwarf stars of spectral classes F–M

ANSGAR REINERS¹ AND MATHIAS ZECHMEISTER¹

¹*Institut für Astrophysik
Friedrich-Hund Platz 1
D-37077 Göttingen, Germany*

ABSTRACT

The determination of extrasolar planet masses with the radial velocity (RV) technique requires spectroscopic Doppler information from the planet’s host star, which varies with stellar brightness and temperature. We analyze Doppler information in spectra of F–M dwarfs utilizing empirical information from HARPS and CARMENES, and from model spectra. We come to the conclusions that an optical setup (*BVR*-bands) is more efficient than a near-infrared one (*YJHK*) in dwarf stars hotter than 3200 K.

We publish a catalogue of 46,480 well-studied F–M dwarfs in the solar neighborhood and compare their distribution to more than one million stars from Gaia DR2. For all stars, we estimate the RV photon noise achievable in typical observations assuming no activity jitter and slow rotation. We find that with an ESPRESSO-like instrument at an 8m-telescope, a photon noise limit of 10 cm s^{−1} or lower can be reached in more than 280 stars in a 5 min observation. At 4m-telescopes, a photon noise limit of 1 m s^{−1} can be reached in a 10 min exposure in approx. 10,000 predominantly sun-like stars with a HARPS-like (optical) instrument. The same applies to ~3000 stars for a red-optical setup covering the *RIz*-bands, and to ~700 stars for a near-infrared instrument. For the latter two, many of the targets are nearby M dwarfs. Finally, we identify targets in which Earth-mass planets within the liquid water habitable zone can cause RV amplitudes comparable to the RV photon noise. Assuming the same exposure times, we find that an ESPRESSO-like instrument can reach this limit for 1 M_⊕ planets in more than 1000 stars. The optical, red-optical, and near-infrared configurations reach the limit for 2 M_⊕ planets in approximately 500, 700, and 200 stars, respectively.

Keywords: catalogs — instrumentation: spectrographs — planets and satellites: detection — stars: low-mass — stars: solar-type — techniques: radial velocities

1. INTRODUCTION

The search for planets around other stars, the characterization of other planetary systems, and the quest for other planets similar to Earth are motivation for a broad range of astronomical research. During the last decades, astronomical techniques improved so that today we know about the existence of thousands of planets, and for many we can determine their masses, sizes, and potential atmospheric composition. A number of complementary techniques exist to obtain information about planets and their characteristics (e.g., [Perryman 2014](#)). Most successful (in number of planet discoveries) are the transit technique that, among other parameters, measures a planet’s size, and the radial velocity (RV) technique that determines the planet’s (projected) mass. Ideal targets are those that can be measured with both the RV and the transit technique. A large number of systems applicable to both methods is expected from the satellite transit missions TESS ([Ricker et al. 2015](#)) and PLATO ([Rauer et al. 2014](#)).

The mass of a planet is determined via reflex motion of the star caused by an orbiting planet. Typical velocities of the star’s motion are several ten m s^{−1} for giant planets (12 m s^{−1} for Jupiter in the solar system), and several cm s^{−1} for terrestrial planets with masses similar to Earth (9 cm s^{−1} for Earth around the Sun). Current instrumental

limitations together with intrinsic stellar variability limits the RV technique to planets that cause stellar velocity amplitudes on the order of 1 m s^{-1} or larger (Fischer et al. 2016). Instruments like ESPRESSO (Pepe et al. 2014; Hogg et al. 2019) aim for the 10 cm s^{-1} -limit, and a new generation of spectrographs at telescopes beyond the 10m-class are planned with similar performance goals (Marconi et al. 2016; Szentgyorgyi et al. 2016).

With the RV method, planets are easier to detect if they orbit less massive stars. Lower-mass dwarf stars are smaller than more massive stars, and they have cooler surface temperatures. Thus, they are significantly fainter than warmer stars, and they show a very different spectral energy distribution exhibiting more flux at longer wavelengths. They generally show more spectral features because of molecular absorption. The question about the minimum detectable planet mass around any given star is therefore not easily answered. This is the topic of this paper.

The RV precision achievable in a stellar spectrum depends on the number of photons (or the signal-to-noise ratio, SNR) and the amount of spectroscopic information, i.e., the presence of spectral features. The RV information content of stellar spectra at visible wavelengths was discussed for example by Connes (1985); Butler et al. (1996), and Bouchy et al. (2001). They demonstrated that sun-like stars are ideal targets for RV determination at optical wavelengths. After the realization that the possibility of life on planets around M dwarfs cannot be generally ruled out (Tarter et al. 2007; Scalo et al. 2007), they became a second focus of RV surveys because smaller planets can be discovered around them. Also, low-mass dwarfs are the most numerous stars in our galactic neighborhood (Henry et al. 2006, 2016). Therefore, growing effort is spent to search for our closest neighbor planets with several RV instruments (Wright & Robertson 2017). Additional motivation comes from the expectation of transiting planets discovered with TESS, and it is important to identify the optimal strategy for RV survey and follow-up observations. Cloutier et al. (2018a) presented a specialized calculation of the total observing time required to measure planet masses from the expected TESS planet yield. In addition to photon noise, they took into account other mechanism causing RV noise including stellar activity. This so-called RV jitter acts as an additional source of noise that can be estimated from Ca activity (e.g., Wright 2005; Santos et al. 2000), photometric flicker (Cegla et al. 2014), or measurements of stellar rotation (Astudillo-Defru et al. 2017). The amplitude of RV jitter is expected to depend on wavelength, which can be useful to distinguishing between Keplerian motion and the stellar activity in RV measurements (Zechmeister et al. 2018). However, the wavelength dependence of stellar activity on RV measurements is not well understood. Temperature spots are expected to cause RV jitter that is smaller at longer wavelengths because of diminished contrast between hot and cool regions (e.g., Martín et al. 2006; Huélamo et al. 2008; Reiners et al. 2010). Zeeman broadening, on the other hand, could lead to an increase of RV jitter with wavelength (Reiners et al. 2013). Cloutier et al. (2018a) therefore chose to implement a wavelength independent term for RV jitter. They highlight the comparable performance of optical and near-IR spectrographs albeit they are not considering spectrographs that cover the red optical wavelength range between 700 and 900 nm.

Identifying the best strategy for RV measurements in low-mass stars was hampered by the difficulty of synthesizing high-resolution spectra including all relevant molecular features, and by the lack of high-resolution infrared observations. Investigation of RV information carried out by, e.g., Reiners et al. (2010); Rodler et al. (2011); Bottom et al. (2013); Plavchan et al. (2015); Beatty & Gaudi (2015); Figueira et al. (2016), showed that the RV observations in M dwarfs should focus on wavelengths redder than 600–700 nm but their results depended on the models’ assumptions. Artigau et al. (2018) employed observations of Barnard’s star (M4V) obtained with HARPS, ESPADONS, and CRIRES to test the radial velocity content of M dwarf spectra. Reiners et al. (2018) determined the amount of RV information in M dwarf spectra between the *V*- and *H*-bands from observations of 324 stars obtained with the CARMENES instrument (Quirrenbach et al. 2016). In this paper, we revisit the radial velocity content of M dwarf spectra, and we add empirical information about M dwarf and hotter star spectra at optical wavelengths. As our main product, we compute the RV precision limit set by photon noise that can be reached with any (ideal) spectrograph and target brightness for an extensive sample of F–M dwarf stars.

We define a sample of stars with well characterized properties in Section 2, and we discuss in Section 3 how the values of RV precision are calculated. In Section 4, we introduce our RV precision catalogue, and we discuss the performance and the potential of different instrument designs regarding the discovery of low-mass planets. In Section 5, we look into the detectability of planets inside the liquid water habitable zone. As a tool for optimizing instrument design, and planning RV observations, we provide an online-calculator for the RV precision achievable for a given star and instrument setup (see Section 3).

2. THE STELLAR SAMPLE

In our sample, we include catalogues with main sequence stars of spectral types F–M. We focus on catalogues with precise information about surface temperature and stellar mass. We summarize the catalogues included in our work in Table 1 where we provide the numbers of stars as well as temperature and brightness ranges. For stars contained in more than one catalogue, we give preference to the publications in the order as listed in Table 1. For F-, G-, and K-dwarfs, we include *The Catalog of Earth-Like Exoplanet Survey Targets* (Chandler et al. 2016), *The Geneva-Copenhagen survey of the Solar neighbourhood* (Nordström et al. 2004), and the catalogue on *Spectral Properties of Cool Stars* (Brewer et al. 2016). For cooler stars, data are taken from *The catalogue of nearby cool host-stars* (Gaidos et al. 2014), *The SPIRou Input Catalogue* (Fouqué et al. 2018), and *The Near-Infrared Spectroscopic Survey of 886 Nearby M Dwarfs* (Terrien et al. 2015). These catalogues all provide spectroscopic determinations of stellar temperature together with magnitudes in different filters. Fouqué et al. (2018) provide H -magnitudes but no J -magnitudes and we approximate $J = H$. We neglect five of the 2974 stars from Gaidos et al. (2014), because they are reported to have extremely low temperatures that appear to be outside the range for which the derived parameters from that work are valid. We complement this information with a sample of very late-M dwarfs by Reiners & Basri (2009), for which we estimate T_{eff} from spectral type according to the relations provided in Kenyon & Hartmann (1995) and Golimowski et al. (2004). Overall, our catalogue contains 46,480 stars from these detailed catalogues. Targets of the CARMENES input catalogue (Reiners et al. 2018) are almost all contained in the list of catalogues above and therefore not explicitly added.

Table 1. Stellar catalogues used for this study prioritized from top to bottom. The second column provides the number of stars adopted from each catalogue. Numbers in brackets show the total numbers of stars given in each catalogue.

Catalog	# stars	T_{eff} range	V range	J range
Chandler et al. (2016)	37354	3042 ... 7199	2.4 ... 13.7	
Nordström et al. (2004)	4782 (14695)	4613 ... 7396	0.4 ... 12.7	
Brewer et al. (2016)	500 (971)	4702 ... 6674	1.7 ... 10.0	
Gaidos et al. (2014)	2969	2700 ... 4803	6.7 ... 17.8	3.9 ... 9.0
Fouqué et al. (2018)	172 (447)	2656 ... 4718	6.9 ... 16.6	3.3 ... 12.3
Terrien et al. (2015)	642 (886)	3276 ... 4523	6.8 ... 15.9	3.9 ... 12.4
Reiners & Basri (2009)	63	2350 ... 2620		8.9 ... 13.3
Gaia DR 2	1188603	3344 ... 8000	3.0 ... 12.0	

We use distances from Gaia DR2 (Gaia Collaboration et al. 2016, 2018) for all stars for which Gaia DR2 reports significant parallax measurements (2σ). Furthermore, we selected more than 1 Million targets from Gaia DR2 data using temperature estimates from Andrae et al. (2018) with apparent Gaia-magnitudes brighter than $g = 12$ mag. For our magnitude plots, we approximate $g = V$. Although these temperatures are of much lower precision than the spectroscopically determined ones, we include them in our analysis to provide an overview about the distribution of stars that is independent of the selected catalogues.¹

We show the distribution of stars from these catalogues as a function of temperature in Fig. 1. Except for Gaia DR2, the catalogues reveal an obvious lack of K-dwarfs with temperatures between 4000 K and 5000 K because most of the detailed spectroscopic work has been done for either M- or G-dwarfs. The distribution of stars in Gaia DR2 shows that this is a systematic feature of the F–K catalogues; most of the volume-limited RV survey samples include only very few K-dwarfs.

For the calculation of planetary mass detection limits, we also need to estimate the mass of the star. For most of the stars, mass estimates are provided in the catalogues. For the stars from Fouqué et al. (2018) and Reiners & Basri (2009), we estimate mass from temperature according to the 2 Gyr evolutionary track from Baraffe et al. (1998). We did not estimate masses for the Gaia DR2 data because the uncertainties would be too high for a meaningful

¹ We do not provide values of RV photon noise for the Gaia DR2 targets in Table 5, because they have rather large uncertainties.

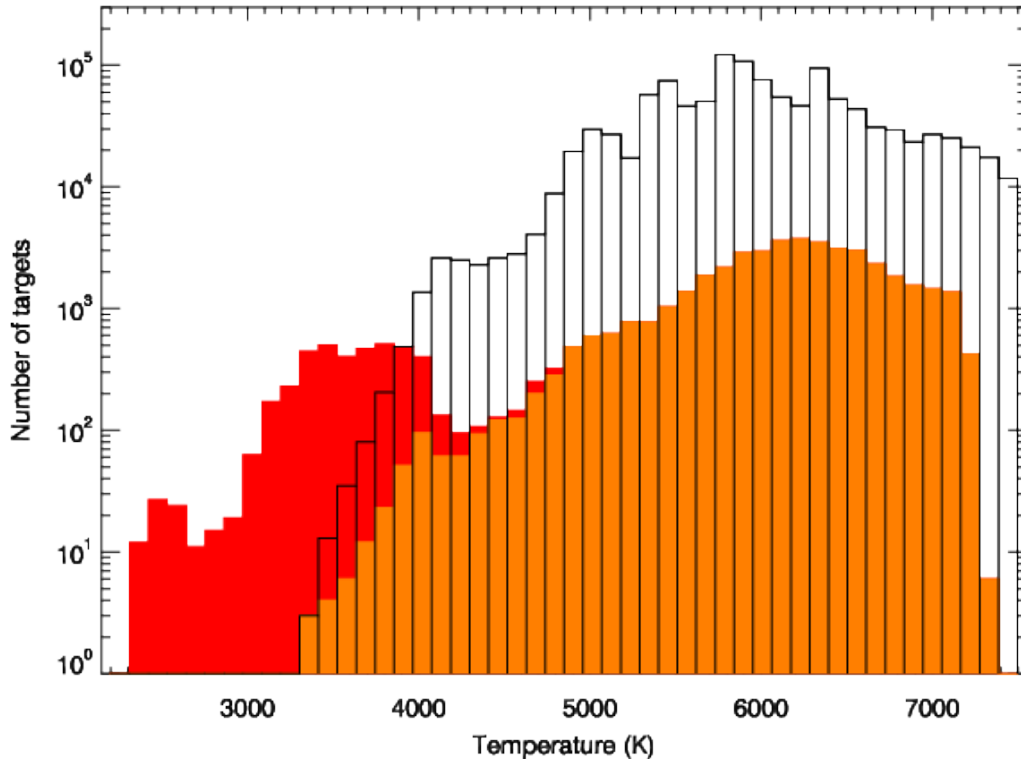


Figure 1. Histogram of the stars contained in the spectroscopic catalogues from Table 1. Stars from F-, G-, and K-star catalogues are shown in orange (Chandler et al. 2016; Nordström et al. 2004; Brewer et al. 2016). Stars from the cool dwarf catalogues are added cumulatively in red (Gaidos et al. 2014; Fouqué et al. 2018; Terrien et al. 2015; Reiners & Basri 2009). The Gaia DR2 sample is overplotted with no color filling.

investigation. An additional factor for the estimate of RV precision is projected rotation velocity $v \sin i$.² For our calculations, we do not include the effect of rotational broadening because its consequences are relatively small for the majority of stars that are slow rotators, and information on $v \sin i$ are missing for large parts of our targets. The assumption of slow rotation is not valid for mid- and late-M dwarfs (e.g., Jeffers et al. 2018). Thus, our estimates of RV photon noise are lower bounds for the RV precision that can be achieved. For the calculation of the habitable zone distance, we also need the luminosity of the star. If luminosity is not provided in the catalogue, we estimate its value from temperature and radius. In catalogues where the radius is not provided either, we estimate radius from stellar mass assuming $M/M_{\odot} = R/R_{\odot}$, which is a reasonable approximation for dwarf stars (Demory et al. 2009).

We show the V -magnitude of all stars in our sample as a function of temperature in the left panel of Fig. 2, and we plot temperature as a function of distance in the right panel of that figure. The two figures provide an orientation about the amount of stars in the solar neighborhood and about their apparent brightness. For comparison, we include information on stars for which extrasolar planets are reported on *The Exoplanet Encyclopedia*³ using the stellar parameters provided there. For these stars, we chose to plot both values from our spectroscopic catalogues (Table 1) and those from exoplanet.eu. Thus, the stars from exoplanet.eu may be plotted twice but the parameters given in the literature are not necessarily identical.

3. DETERMINING RADIAL VELOCITY PHOTON NOISE

The fundamental limit for the RV precision that can be achieved from an observation of any given star is the RV photon noise. In order to estimate the RV photon noise, we need to specify the RV information content for the spectrum

² For resolved spectral lines and rotationally dominated line broadening, RV photon noise scales proportional to $(v \sin i)^{1.5}$. In practice, the scaling is less steep for most sun-like and cooler stars with $v \sin i < 10 \text{ km s}^{-1}$ and depends on spectral resolution (see Fig. 7 in Reiners et al. 2010).

³ <http://exoplanet.eu>

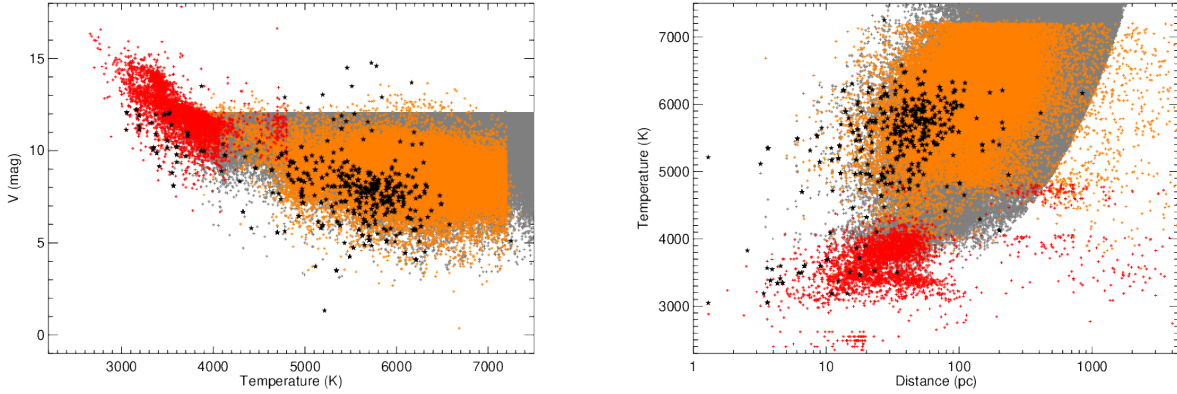


Figure 2. Sample of stars used for this work with the colors for sun-like star catalogues in orange and the cool dwarf catalogues in red, respectively, as in Fig. 1. Stars from Gaia DR2 and Andrae et al. (2018) are shown in grey. Black stars show known planet hosts from exoplanet.eu. *Left:* Apparent brightness as a function of spectroscopic temperature. *Right:* Temperature as a function of distance.

of a star of given temperature, and its signal-to-noise ratio, SNR (Connes 1985; Butler et al. 1996; Bouchy et al. 2001). The RV precision achieved in an actual observation can further be deteriorated by additional line broadening, in particular by stellar rotation and activity. Line broadening diminishes the amount of spectroscopic features and its effect can be compensated with higher SNR (longer exposures). Stellar activity can be a source of additional (additive) noise that cannot be overcome by longer exposures alone but must be addressed by modeling the effect using additional information (e.g., Aigrain et al. 2012; Haywood et al. 2016; Dumusque 2018; Collier Cameron et al. 2019). Stellar metallicity influences the amount of spectral features and also the colors of stars and therefore the distribution of SNR across wavelengths. In our estimates, we neglect the influence of metallicity. For the model calculations, including the effect of metallicity would be relatively straightforward. Comparison to observed spectra, however, is hampered by uncertainties of the observed stars’ metallicity, particularly in low-mass stars where the model spectra are known to be imprecise (see Artigau et al. 2018; Passegger et al. 2018). Relative to the other effects considered, metallicity is expected to create only minor deviations for the stars considered in this paper.

Our goal is to calculate RV photon noise for observations taken with visual light and infrared spectrographs. For this, we investigate the RV information at wavelengths $\lambda = 380\text{--}2380\text{ nm}$. We limit our study to stars between temperatures $T_{\text{eff}} = 2800\text{ K}$ and 7000 K . While RV information can be directly computed from synthetic models, Artigau et al. (2018) and Reiners et al. (2018) showed that model spectra do not always correctly represent the abundance and depth of absorption features. This is particularly important for absorption from molecular bands in cool stars. Artigau et al. (2018) investigated HARPS, ESPADONS, and CRIRES spectra of Barnard’s star (M4). Reiners et al. (2018) employed data from the CARMENES survey to determine RV photon noise across the M dwarf spectral range (M0–M9). In general, the results of both studies agree very well; they both conclude that the wavelength range around $700\text{--}900\text{ nm}$ (I -band) provides the most accurate measurements. However, there are some significant differences at other wavelength bands that we discuss in the following.

In order to construct a consistent set of empirical photon noise limits across a variety of stellar temperatures and wavelengths, we make use of several thousand spectra observed with the HARPS and CARMENES instruments. For M-stars and wavelengths $550\text{--}1780\text{ nm}$, we use the RV photon noise values from Reiners et al. (2018) from the CARMENES survey for planets around M dwarfs. To this data, a telluric mask excluding atmospheric features deeper than 5% was applied (see Zechmeister et al. 2018). For hotter stars and wavelengths $380\text{--}650\text{ nm}$, we calculate the RV photon noise from ESO-HARPS archival data from 383 stars. For each star, we take the available archive data from HARPS-DRS⁴ including SNR. From this data, we determine the amount of RV information for each individual order and calculate values of RV precision for stars with temperatures between $T_{\text{eff}} = 3200\text{ K}$ and 6000 K . For all stars and wavelength ranges in our grid, we additionally compute RV information from synthetic PHOENIX model spectra (Husser et al. 2013) adapted to the instrument resolutions. For this, we choose to exclude pixels with more

⁴ <http://www.eso.org/sci/facilities/lasilla/instruments/harps.html>

than 10 % telluric absorption. We emphasize that there is a conceptual difference between the RV photon noise limits estimated from theoretical as well as observed spectra (as done for HARPS and model spectra in [Artigau et al. 2018](#), and here for model spectra only), and the empirically determined RV precision (calculated for CARMENES data in [Reiners et al. 2018](#), and here for HARPS data). For the empirical case, we use the actual uncertainties derived from the determination of RVs. We refer to [Zechmeister et al. \(2018\)](#) and [Reiners et al. \(2018\)](#) for a detailed discussion. Because of major uncertainties, e.g., in the scaling of SNR (or the brightness of stars as a function of wavelength), the treatment of telluric lines, in metallicities, and in the synthetic models, we expect some disagreement between the RV photon noise limits from different sources. Our comparison should help to identify these uncertainties and potential problems in RV precision estimates.

The results about our RV photon noise limits and empirical precision estimates for different stellar types are shown in Fig. 3. We show our results from CARMENES, HARPS, and model spectra with different symbols for comparison, and we include results from [Artigau et al. \(2018\)](#) for Barnard’s star. The plotted values of RV photon noise are assuming a SNR of 100 per pixel in the *V*-band for $R = 100,000$.⁵ For the synthetic model calculations, we use a 2.5-pixel sampling. Note that this assumption leads to extremely low photon noise values (very high precision) for very cool (M-type) stars. Observations of M stars typically do not achieve such high *V*-band SNRs, and [Reiners et al. \(2018\)](#) provide RV photon noise for SNR = 150 in the *J*-band. We scale the CARMENES values assuming that the *J*-band SNR for an object of a given *J*-magnitude is 72 % of the *V*-band SNR from an object that has the same magnitude in the *V*-band.⁶ From [Artigau et al. \(2018\)](#), we adopt their results for the 2 % telluric absorption limit and scale the numbers from their Table 4 by a factor of 7.5, which is approximately the ratio between the SNR of a M4 star in the *V*-band and in the *J*-band (see [Reiners et al. 2018](#), Fig. 7). To account for rotational broadening in the synthetic model spectra, we assign rotation rates to our model stars, which are the lowest ones typical for a given stellar mass (thus allowing the highest possible RV precision). We estimate the upper envelope of rotation periods as a function of stellar mass from Eq. (6) in [Newton et al. \(2017\)](#) and Fig. 8 in [Reinhold et al. \(2013\)](#), and we broaden our synthetic spectra before calculating RV photon noise. Inactive dwarf stars cooler than the Sun typically rotate at rotation rates of several 10 d or slower, which is less than $1\text{--}2\text{ km s}^{-1}$ and negligible for our calculations. More massive stars, however, rotate substantially faster, which leads to a significant decrease in RV precision in these stars. The RV photon noise for the case $T = 7000\text{ K}$ is not shown in Fig. 3. The approximate lower limit of rotational velocities for these stars is $v_{\text{eq}} = 70\text{ km s}^{-1}$, and the typical RV photon noise limit is several 10 m s^{-1} (Table 2). We note that stars observed under low inclination angles may show lower projected velocities, $v \sin i$, and therefore show lower RV photon noise.

Our first observation in Fig. 3 is that information on RV photon limits and empirical values on RV precision from different sources are consistent for most of our parameter space. The high overall agreement of the *absolute* values from different methods demonstrates that understanding of RV photon noise has become relatively robust. In particular, values where CARMENES and HARPS results are available, i.e., at $\lambda = 600\text{ nm}$ and $T_{\text{eff}} = 3200, 3700\text{ K}$, the values agree very well. This is an important validation of our method combining CARMENES and HARPS measurements. The results from spectral models also show remarkably similar trends in wavelength and temperature; differences from the measured values are smaller than a factor two with very few exceptions. The main reason for discrepancies in the coolest stars is probably incomplete understanding of line formation, in particular for molecular lines in M dwarfs (see [Reiners et al. 2018](#); [Artigau et al. 2018](#)), and treatment of telluric lines.

The comparison between the results for Barnard’s star from [Artigau et al. \(2018\)](#) and our empirical case for 3200 K also shows very good agreement in general. At wavelengths between 550 nm and 900 nm, and in the *J*-band, the values only differ by a few percent. In the *Y*-band around $1\text{ }\mu\text{m}$, our CARMENES data indicate significantly lower RV photon noise than the CRIRES results, and in the *H*-band, the CRIRES results suggest lower RV photon noise than the CARMENES results. As discussed in [Artigau et al. \(2018\)](#), this has implications for the design of infrared spectrographs, in particular whether RV infrared surveys should concentrate on the *Y*-band or the *H*- and *K*-bands. We cannot provide a clear answer as to why our results are different from theirs at infrared wavelengths. The difference in the *H*-band can perhaps be explained by differences in SNR scaling and in the exact definition of the wavelength band used for the computations; Fig. 2 in [Artigau et al. \(2018\)](#) shows that most of the RV information in the *H*- and the *K*-bands is located at the extreme ends of the two bands. For the *Y*-band, [Artigau et al. \(2018\)](#) argue that the

⁵ For the model spectra, we define the SNR of a wavelength range as the 90th-percentile of the SNR for all pixels within that range.

⁶ The square-root of the ratio between the number of photons from a 10,000 K blackbody at 550 nm and 1215 nm, assuming constant instrument resolution, is 0.72. The number of photons per resolution element is proportional to the Planck function in units per wavelength (λ^{-1}) times λ^2 .

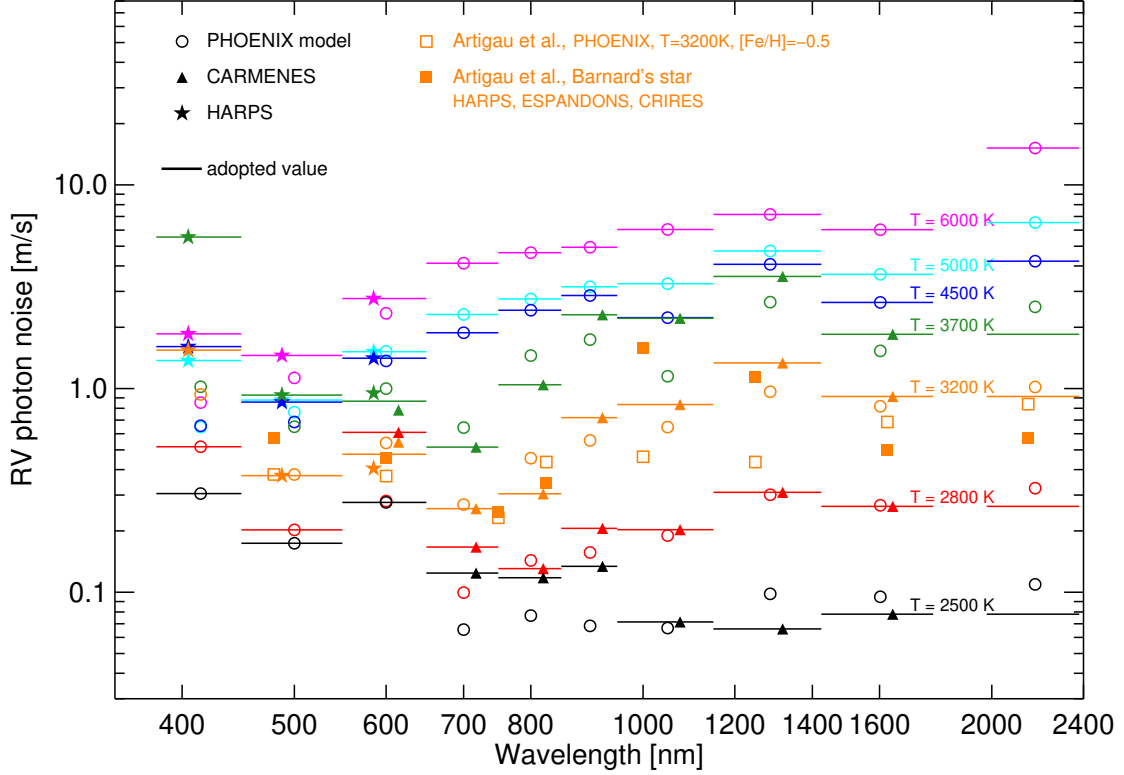


Figure 3. Radial velocity photon noise as a function of wavelength for spectra from stars of different temperatures observed with SNR = 100 in the V-band. We show RV photon noise from difference sources: predicted values from spectral models (open circles), CARMENES empirical values (triangles), HARPS empirical values (stars), and model predictions (open squares) as well as empirically determined values (solid squares) for Barnard’s star from [Artigau et al. \(2018\)](#). Values adopted for our RV precision calculations are shown as horizontal lines that also indicate our wavelength chunks (Table 2). Not included are results for $T = 7000$ K (see text).

models overpredict the achievable RV precision in Barnard’s star by a factor of roughly three, which we cannot confirm. A factor of three in RV photon noise corresponds to almost an order of magnitude difference in spectral information, which means a model overprediction of line depth or density. The spectral atlas of Luyten’s star (M3.5) displayed in Appendix A of [Reiners et al. \(2018\)](#) shows that the observed lines are in fact generally weaker than predicted in this star. However, in the Y-band, most of the molecular absorption appears at the predicted location indicating that a correction by a factor of three is unlikely. Interestingly, the comparison between our model spectra noise limits and those from [Artigau et al. \(2018\)](#) also shows some significant differences, despite both studies use identical models. We cannot explain this discrepancy but we suspect that the choice of wavelength regions included in the calculation and the way the distribution of SNR is treated across wavelengths are major sources of uncertainty. In our coolest example ($T = 2500$ K), RV photon limits differ between our model calculations and empirical values in the range 700–900 nm. Model spectra do show an overabundance of molecular absorption in comparison to observed spectra (see Appendix A in [Reiners et al. 2018](#)), but since the empirical RV estimates rely on stars that are very faint, they may also partly be affected by read-out noise in this wavelength range.

From the information shown in Fig. 3, we create a grid of RV precision values for dwarf stars of spectral types F–M. We adopt empirical values where available from CARMENES and/or HARPS, and we rely on predictions from PHOENIX spectral models otherwise. We have no empirical information about the K-band from CARMENES and assume that in M dwarfs ($T < 4000$ K) the spectral information content of the K-band is similar to the H-band (see [Rodler et al. 2011](#); [Figueira et al. 2016](#); [Artigau et al. 2018](#)). For hotter stars, we rely on our modelling results. At wavelengths and temperatures for which CARMENES and HARPS information are both available, we take the average

Table 2. Grid of radial velocity precisions for dwarf stars at visual and infrared wavelengths. Values are given for an SNR of 100 at $\lambda = 550$ nm (V -band) and $R = 100,000$.

T_{eff}	Wavelength range (nm)									
	380	450	550	650	750	850	950	1150	1425	1980
	450	550	650	750	850	950	1150	1425	1780	2380
RV photon noise (m s^{-1})										
7000	33.08	52.75	115.48	138.96	148.73	100.72	110.38	94.35	117.58	168.04
6000	1.86	1.45	2.77	4.13	4.65	4.94	6.04	7.16	6.03	15.17
5000	1.37	0.88	1.52	2.31	2.75	3.16	3.27	4.74	3.64	6.53
4500	1.61	0.86	1.41	1.88	2.42	2.86	2.23	4.07	2.65	4.22
3700	5.55	0.93	0.87	0.52	1.04	2.30	2.21	3.55	1.85	1.85
3200	1.54	0.37	0.48	0.26	0.30	0.72	0.83	1.34	0.91	0.91
2800	0.52	0.20	0.61	0.17	0.13	0.21	0.20	0.31	0.26	0.26
2500	0.30	0.17	0.28	0.12	0.12	0.13	0.07	0.07	0.08	0.08

Table 3. Same as Table 2 but for an SNR of 150 at $\lambda = 1200$ nm (J -band).

Wavelength range (nm)								
	550	650	750	850	950	1150	1425	1980
	650	750	850	950	1150	1425	1780	2380
T_{eff}	RV photon noise (m s ⁻¹)							
3700	1.49	0.98	1.98	4.37	4.20	6.75	3.51	3.51
3200	1.95	0.92	1.09	2.57	2.98	4.77	3.27	3.27
2800	5.18	1.42	1.11	1.75	1.72	2.63	2.24	2.24
2500		3.69	3.50	3.98	2.12	1.96	2.32	2.32

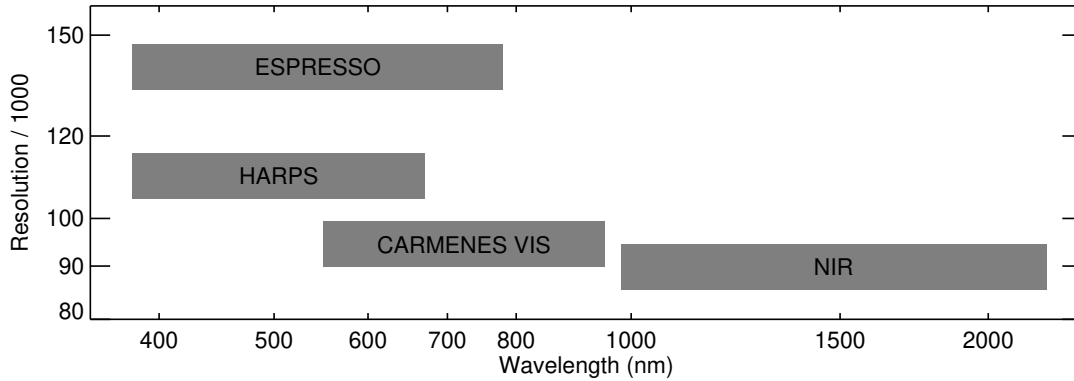


Figure 4. Visualization of resolution and wavelength coverage of the four spectrograph designs used as examples.

of the two. As mentioned earlier, we generally scale RV photon noise based on stellar V -magnitudes. For M dwarfs we also provide values based on J -magnitudes. The grid values are summarized in Tables 2 and 3.

Table 4. Spectrograph parameters as used for the RV precision estimates.

Instrument	λ (nm)	R	rel. SNR	Exp. time
ESPRESSO	380 – 780	140,000	2	5 min
HARPS	380 – 670	110,000	1	10 min
CARMENES VIS	550 – 950	94,600	1	10 min
NIR	980 – 2440	90,000	1.2	10 min

4. RADIAL VELOCITY PHOTON NOISE CATALOGUE

For the stars in the catalogues introduced in Sect. 2, we compute in this Section individual RV photon noise limits expected in a typical observation for a few typical spectrograph designs. In Sect. 5, we estimate minimum masses of planets detectable in the stars’ liquid water habitable zones following from the RV photon noise. In addition to our catalogue, we provide an online tool with the relevant formulae. The user can compute RV precision limits for individual stars or star lists and for specific observational configurations.⁷

4.1. Spectrographs

We compute RV precision estimates for four example spectrograph designs; (1) an ultra-high resolution spectrograph at an 8-m telescope covering a very wide wavelength range like ESPRESSO (Pepe et al. 2014), (2) the HARPS-design (Mayor et al. 2003) with very high resolution at visual wavelengths operating at a 4m-class telescope, (3) a red optical design like CARMENES-VIS (Quirrenbach et al. 2016) fed by a 4m telescope, and (4) a near-infrared (NIR) design covering wavelengths redward of 900 nm like, e.g., CARMENES-NIR (Quirrenbach et al. 2016), SPIROU (Donati et al. 2017), NIRPS (Wildi et al. 2017), and GIANO (Origlia et al. 2014). The parameters are summarized in Table 4 and visualized in Fig. 4. We specify instrument efficiency in terms of SNR relative to HARPS and CARMENES-VIS values; these instruments deliver comparable SNR after identical exposure times on objects of the same brightness. Estimates for ESPRESSO and HARPS instrument throughput are based on ESO exposure time calculators.⁸ CARMENES-VIS estimates are taken from Reiners et al. (2018). Our NIR design SNR estimate is based on a SPIROU estimate (Donati et al. 2017), which is somewhat higher than the CARMENES-VIS and HARPS throughput. For our calculations, we assume an exposure time of 5 min for ESPRESSO and 10 min for the other spectrograph designs. This is an arbitrary choice motivated by typical exposures used at 4m- and 8m-class telescopes for high-precision RV observations. In exposures shorter than a few minutes, solar-like oscillations likely do not average out, in particular in higher-mass stars (Chaplin et al. 2019). For longer exposure times, RV precision scales with $\sqrt{t_{\text{exp}}}$, but exposures should not be longer than a few ten minutes to avoid large systematic errors from barycentric motion (e.g., Tronsgaard et al. 2019).

4.2. RV photon noise

In order to estimate the RV photon noise for the stars of our sample, we scale the SNR according to stellar brightness (and RV photon noise $\propto 1/\text{SNR}$). For stars from the F–K dwarf catalogues, we scale SNR according to V -band magnitudes (Table 2). For stars from Gaia DR2 we assume $\text{Gaia-}g = V$. For stars cooler than 3800 K, we do not rely on the V -band magnitudes alone because these stars are very faint at optical wavelengths and not all catalogues provide V -magnitude; we use the J -magnitudes instead (Table 3). If the V -magnitude is available as well, we use it to calculate RV precision at wavelengths shorter than 550 nm. If no V -magnitude is available, we neglect this wavelength range. In our SNR calculations, we include read-out noise of 20 electrons per extracted pixel in the reduced spectrum. This value can differ a lot for different spectrographs, for example spectrographs with image or pupil slicers typically collect more read-out noise than others. Read-out noise can be important at optical wavelengths in low-mass stars, where spectral information is very dense and relatively low values of SNR can still provide high RV precision. For simplicity, we use the term *RV photon noise* although our results can be read-out noise limited in very faint stars.

⁷ <http://www.astro.physik.uni-goettingen.de/research/rvprecision>

⁸ <http://eso.org/observing/etc>

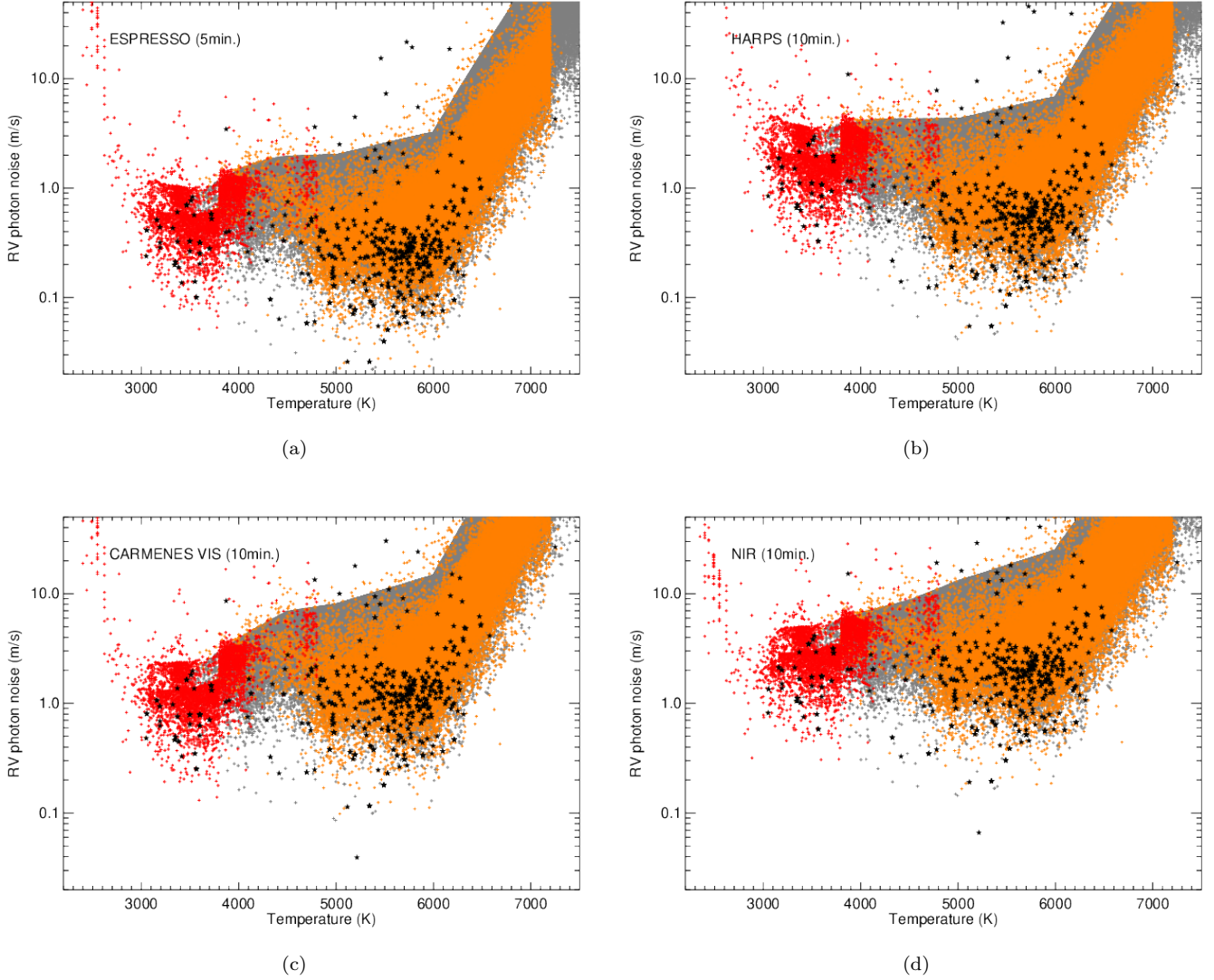


Figure 5. RV photon noise for the stars of our sample estimated for 10 min observations with the spectrograph designs (a) ESPRESSO, (b) HARPS, (c) CARMENES VIS, and (d) NIR, see Table 4. Colors indicate the reference catalogues as in Fig. 2.

The RV photon noise achievable with the four fiducial spectrograph models are shown in Fig. 5. We re-emphasize that these values are theoretical lower limits that are often well below the instrumental or stellar jitter. We also recall that these values are estimates valid for fixed exposure times of 5 and 10 min (Table 4), and that lower photon noise limits can always be achieved through longer exposures. While the absolute values for our example observations can be scaled by adjusting exposure times, the relative performances between stars of different temperatures, and the comparison between instruments of different design, are fixed within the limits of throughput, performance limitations, and uncertainties in our RV noise estimates above as well as its scaling with stellar brightness including a read-out noise-floor. It is therefore very instructive to investigate the temperature-dependent performance of different spectrograph designs. Finally, we note that all our calculations are carried out for the full set of stars regardless of their position on the sky, i.e., they are valid for instruments with similar performance as our spectrographs examples, but not all of the objects are observable from the locations of actually existing instruments.

The distribution of RV photon noise in Fig. 5 shows the consequences from the choice of wavelength coverage. The ESPRESSO design covers the entire optical spectrum between 380 nm and 780 nm. Among the stars available in our catalogues (ca. 3000–7000 K), many of the brightest stars can be observed with RV photon noise limits around 10 cm s^{-1} or better. After 5 min, the ESPRESSO design can collect enough photons to reach an RV noise limit better

than 2 m s^{-1} for almost all stars in our catalogues except for the coolest (and faintest) ones and the hottest stars ($> 6000 \text{ K}$) that are likely rotating too rapidly. Note again that we did not include actual measurements of $v \sin i$ here (see above). The RV photon limits for the other three spectrographs are generally a bit higher because our fiducial ESPRESSO exposures collect about a factor of two more photons (at the same wavelengths).

Like ESPRESSO, the HARPS design also has a spectral resolution well above $R = 10^5$ and covers wavelengths redward of 380 nm , but the cutoff at long wavelengths occurs approximately 110 nm bluer than for the ESPRESSO format. The missing red wavelength range carries a lot of RV information in M dwarfs (Reiners et al. 2018), and its lack is the reason why the HARPS design performs worse in M dwarfs relative to hotter stars in comparison to the ESPRESSO design. The sweet spot of the HARPS design is in the G-dwarfs where some targets provide enough information for RV measurements at the 10 cm s^{-1} level after 10 min. Furthermore, also a large number of M dwarfs can be observed with RV photon noise limits better than 1 m s^{-1} after the same exposure times, which is consistent with the results of, e.g., Mayor et al. (2009); Bonfils et al. (2013); Anglada-Escudé et al. (2013, 2014, 2016).

The two other spectrograph designs in our comparison, the CARMENES VIS and the NIR design, are both optimized for M dwarfs. Their RV photon limits are skewed with respect to the curves from the optical designs like ESPRESSO and HARPS. Dwarfs later than spectral type M5/M6 ($\sim 2800 \text{ K}$) become drastically fainter towards lower temperature, with the result that the SNR of individual exposures becomes very low. Thus, for the conditions simulated here, the RV photon limits in late-M dwarfs ($< 2800 \text{ K}$) for observations at our 4m-class designs are not better than a few m s^{-1} even in the closest objects. Nevertheless, at this temperature, the wavelength coverage of the CARMENES VIS and NIR designs provide significant improvement with respect to the visible-light designs. For the brightest late-M dwarfs on the sky, RV photon limits better than 10 m s^{-1} can be reached within 10 min. Again, we want to emphasize that our RV photon limits are theoretical values that do not take into account stellar jitter and individual values of rotational broadening. Mid- and late-M dwarfs are often rapid rotators with high values of projected rotation velocities, $v \sin i$, as large as a few ten km s^{-1} (e.g., Mohanty & Basri 2003; Reiners et al. 2012). For the selection of targets in an RV survey, the effect of rotational broadening should be taken into account.

4.3. Optical or near-IR?

With our RV noise calculations, we can compare performances of spectrographs designed for different wavelengths. Cloutier et al. (2018a) quantified the observational effort required for RV measurements in TESS targets. They compared an optical HARPS-like design to a near-infrared design covering wavelengths across spectral bands YJH . An important conclusion from their work is that M dwarfs with $T \lesssim 3800 \text{ K}$ are more efficiently observed with near-IR spectrographs than with optical ones. Here, we want to revisit the question whether optical or near-IR spectrographs are more efficient for M-dwarf RV follow-up.

In Fig. 6, we show for each star the ratios between photon noise limits achieved with different spectrograph designs as a function of stellar temperature. In our comparison, we include the optical HARPS-like design covering the BVR bands, the CARMENES-VIS design covering the RIZ bands, and the near-IR design covering $YJHK$. Ratios between the RV noise limits are independent of other design details assuming that all parameters except wavelength coverage are comparable.

The comparison between optical (BVR) and near-IR ($YJHK$) instruments are shown in black in Fig. 6. In sun-like stars, the optical setup outperforms the near-IR one by roughly a factor of four. High values of SNR and the much higher density of spectral features in the blue part of the spectrum favor the instrument design covering shorter wavelengths. In stars of cooler temperature, according to our calculations, the near-IR design is more efficient than the optical design at stellar temperatures $T \lesssim 3200 \text{ K}$. This result is significantly different from the breakpoint at 3800 K reported by Cloutier et al. (2018a) with potentially relevant consequences for RV follow-up projects. It is therefore important to understand the reasons behind this discrepancy. Cloutier et al. (2018a) compared the total observational effort to characterize potential TESS planets. In addition to photon noise, they included other sources of RV jitter, but they chose to not introduce any wavelength dependence in their jitter terms. This means that their comparison of RV noise limits between spectrographs is conceptually not different to ours. The calculations of Cloutier et al. (2018a) were based on the same synthetic model spectra as our model calculations, but they applied the empirical correction factors Artigau et al. (2018) determined for Barnard’s star (M4) to all their calculations. For a more direct comparison between our ratios and the results from Cloutier et al. (2018a), we use their online calculator⁹ to calculate RV photon

⁹ <http://maestria.astro.umontreal.ca/rvfc/>

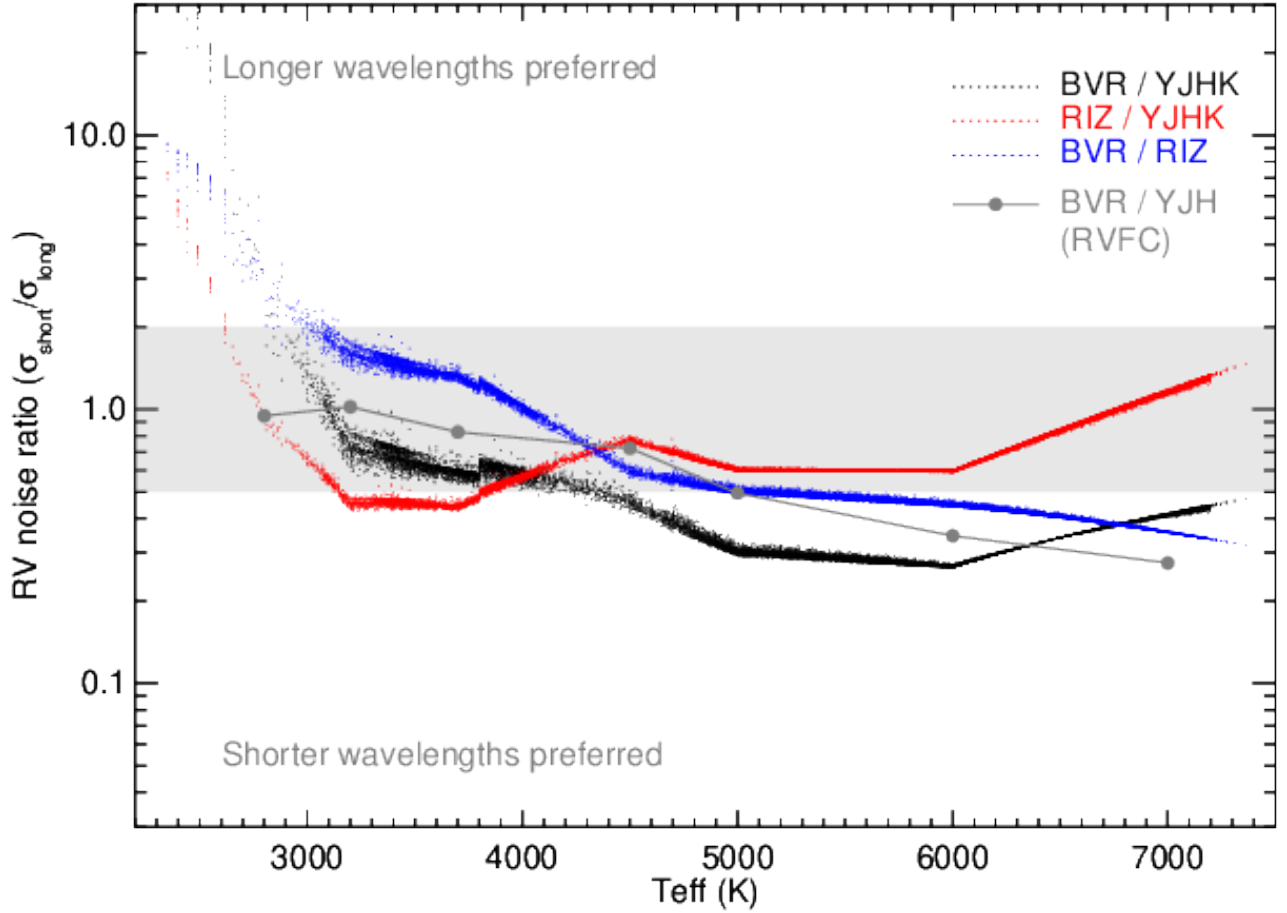


Figure 6. Ratios between RV photon noise achieved in observations of dwarf stars with different spectrograph designs as a function of stellar effective temperature. For each star, black points show the ratio between the performance of a HARPS-like design covering the BVR-bands and a near-IR SPIROU-like design covering YJHK. The red and the blue points show RV noise ratios between a red-optical instrument covering RIZ (like CARMENES-VIS) and the near-IR design, and between the optical and red-optical designs, respectively. The grey circles show results from calculations using the radial velocity follow-up calculator from Cloutier et al. (2018a). Within uncertainties, two spectrographs perform similarly if the ratio is located in the range 0.5–2.0 (grey).

noise limits for seven stars with typical main-sequence parameters. RV noise limits are calculated for the HARPS (optical) and SPIROU (near-IR) spectrograph designs as offered in the tool. We plot the ratios $\sigma_{\text{RV,opt}}/\sigma_{\text{RV,nearIR}}$ as grey circles in Fig. 6. We find that these ratios are very different from the estimated observation efforts reported in Fig. 3 of Cloutier et al. (2018a). Specifically, our calculations predict that the optical and near-IR designs are performing relatively similar in dwarf stars with $T \lesssim 5000$ K. In hotter stars, the optical design outperforms the near-IR by about a factor of three. The near-IR design is not predicted to be significantly more efficient than the optical at stellar temperatures $T \geq 2800$ K, which is the lower temperature limit of the online tool. We suspect that the discrepancy between the RV efficiency estimated in Artigau et al. (2018) and our results from their online tool is caused by read-out noise dominating the results in Artigau et al. (2018), predominantly in the BVR-bands. Their sample includes many relatively faint objects while our seven test objects were chosen to be bright enough to neglect read-out noise. The effect of read-out noise can be seen in the RV noise ratios of our (relatively bright) sample stars in Fig. 6; the (relatively small) scatter in the RV noise at a given temperature is caused by read-out noise.

The optical and near-IR design both do not include the *I*-band, which is the wavelength range carrying most RV information among M dwarfs (see Artigau et al. 2018; Reiners et al. 2018). We also compare the red-optical design (RIZ) to the optical (BVR) and to the near-IR designs (YJHK) in Fig. 6. It is not surprising that the RIZ-design

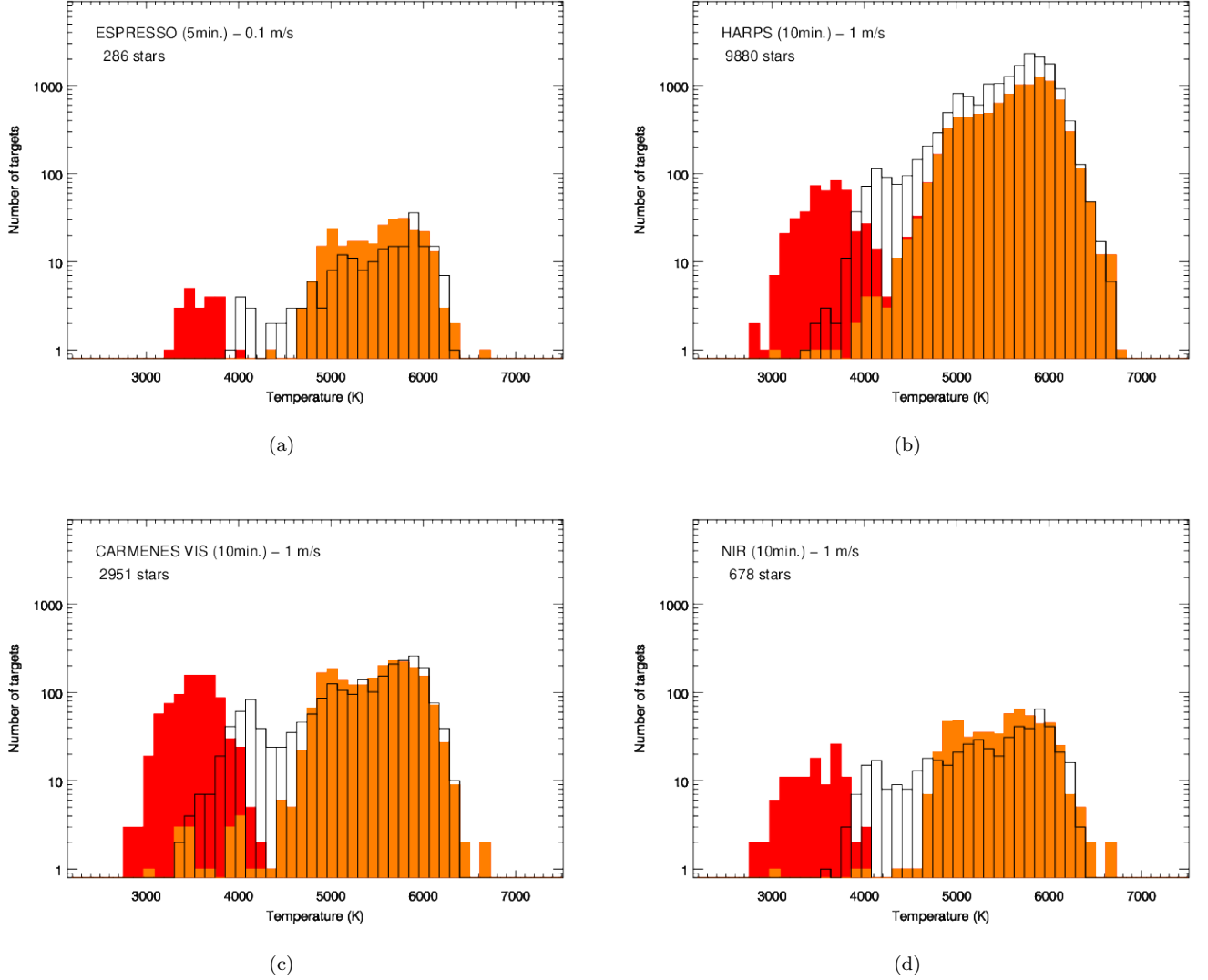


Figure 7. Histograms of the number of stars from the catalogues in Table 1 for which an RV photon limit of 0.1 m s^{-1} (ESPRESSO design – shown in panel a) or 1 m s^{-1} (panels b–d) can be reached within 10 min. Colors indicate stars from different catalogues as in Fig. 2.

(red-optical) is more efficient than the *BVR*-design (optical) in stars with $T_{\text{eff}} \lesssim 4000 \text{ K}$. For the comparison between the *RIZ*-design to the *YJHK*-design (near-IR), one could expect that the redder *YJHK*-design outperforms the bluer *RIZ*-design because of the higher flux density in the near-IR. Nevertheless, as shown for example in Reiners et al. (2018), the much higher information content in the *I*-band, predominantly caused by molecular lines, compensates for this effect. As a result, the red-optical (*RIZ*) design is more efficient than the near-IR (*YJHK*) in M dwarfs with $T_{\text{eff}} \gtrsim 2700 \text{ K}$, i.e., M dwarfs earlier than approximately M7.

4.4. Reaching the 1 m s^{-1} and 10 cm s^{-1} noise limits

An RV precision of 1 m s^{-1} is often the goal of modern spectrograph design, and ESPRESSO was designed with the goal of measuring RV variations on the order of 0.1 m s^{-1} similar to the effect of Earth on the Sun. As discussed above, the time required to reach a given RV photon limit depends on the star’s brightness, the size and efficiency of the telescope, and the spectrograph design. For the example designs of spectrographs we now ask the question for how many stars from our sample a given RV photon limit can be reached after a fixed exposure time.

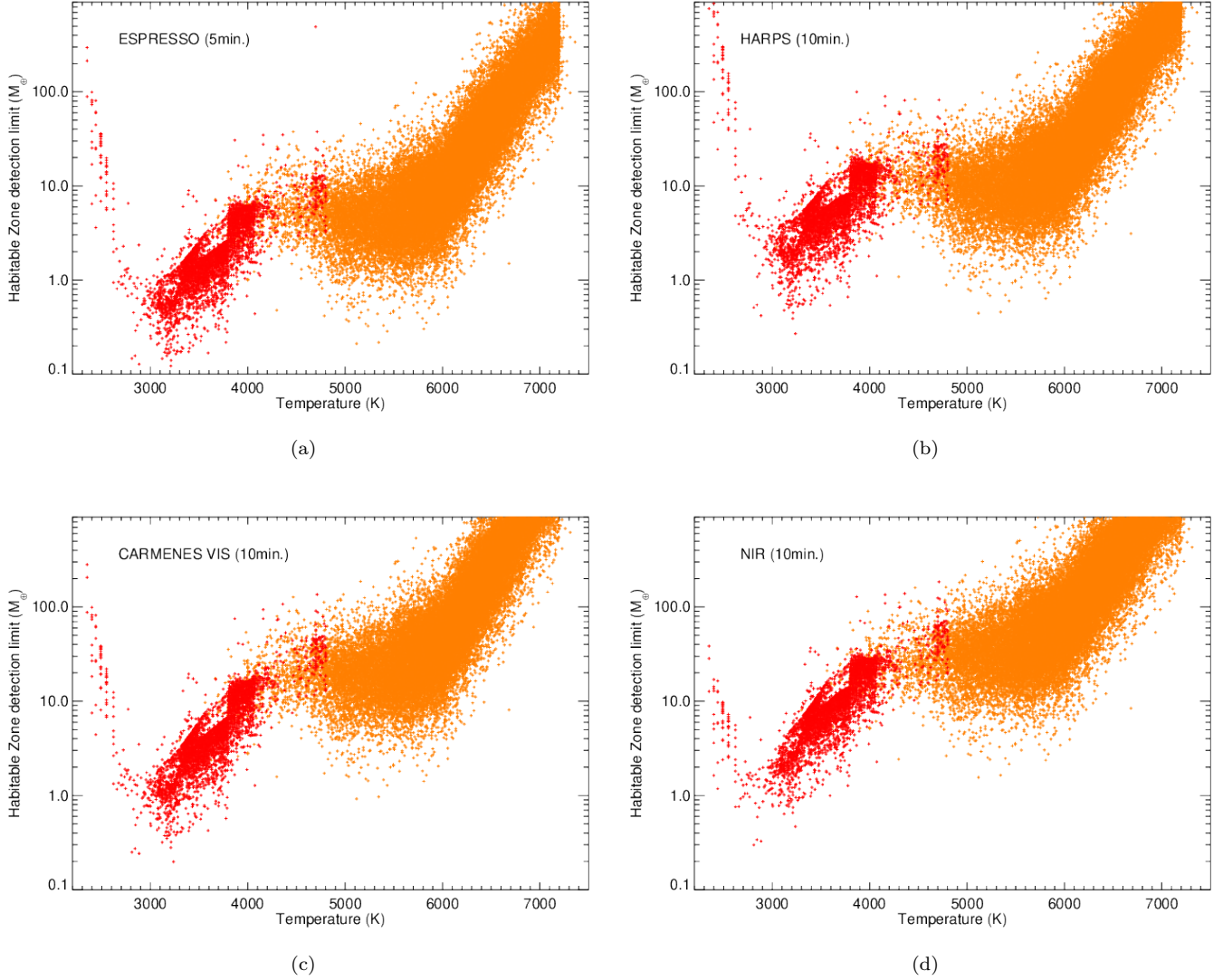


Figure 8. Minimum masses of planets orbiting inside the HZ of stars from our sample that can be detected with the four observational setups as explained in the text. Colors indicate stars from different catalogues as in Fig. 2.

We show in Fig. 7 histograms for the stars in which an RV photon limit of 1 m s^{-1} (0.1 m s^{-1}) can be reached within 10 min (5 min) for the HARPS, CARMENES VIS, and NIR designs (ESPRESSO design). For the ESPRESSO design, we find that 286 stars from our sample are candidates for observations at the 0.1 m s^{-1} level. Most of them are stars with temperatures between 5000 K and 7000 K but there are also some ten stars cooler than 4000 K (spectral types early- to mid-M). Considering the 4m-class instruments, we find that with the HARPS design, 9880 stars from our sample are generally suitable for observations to determine RVs with a photon noise limit better than 1 m s^{-1} within 10 min. Most of these stars are F- and G-type stars. The numbers decrease towards cooler temperatures, and there are several 100 early- to mid-M dwarfs that fulfill the criteria. The CARMENES VIS design is less efficient for stars of spectral type F–K but more efficient in very cool stars. This results in higher numbers of mid- and late-M stars reaching the targeted RV precision. Overall, we find 2951 stars in which a limit of 1 m s^{-1} can be reached in a 10 min exposure. For the NIR design, we find that the 1 m s^{-1} level can be reached in 678 stars. For all cases, we find a lack of targets between 4000 K and 5000 K (K-dwarfs). This type of stars is not well covered by the catalogues we used. Gaia DR2 contains a number of stars that are probably suitable for these measurements.

5. HABITABLE ZONE LIMITS

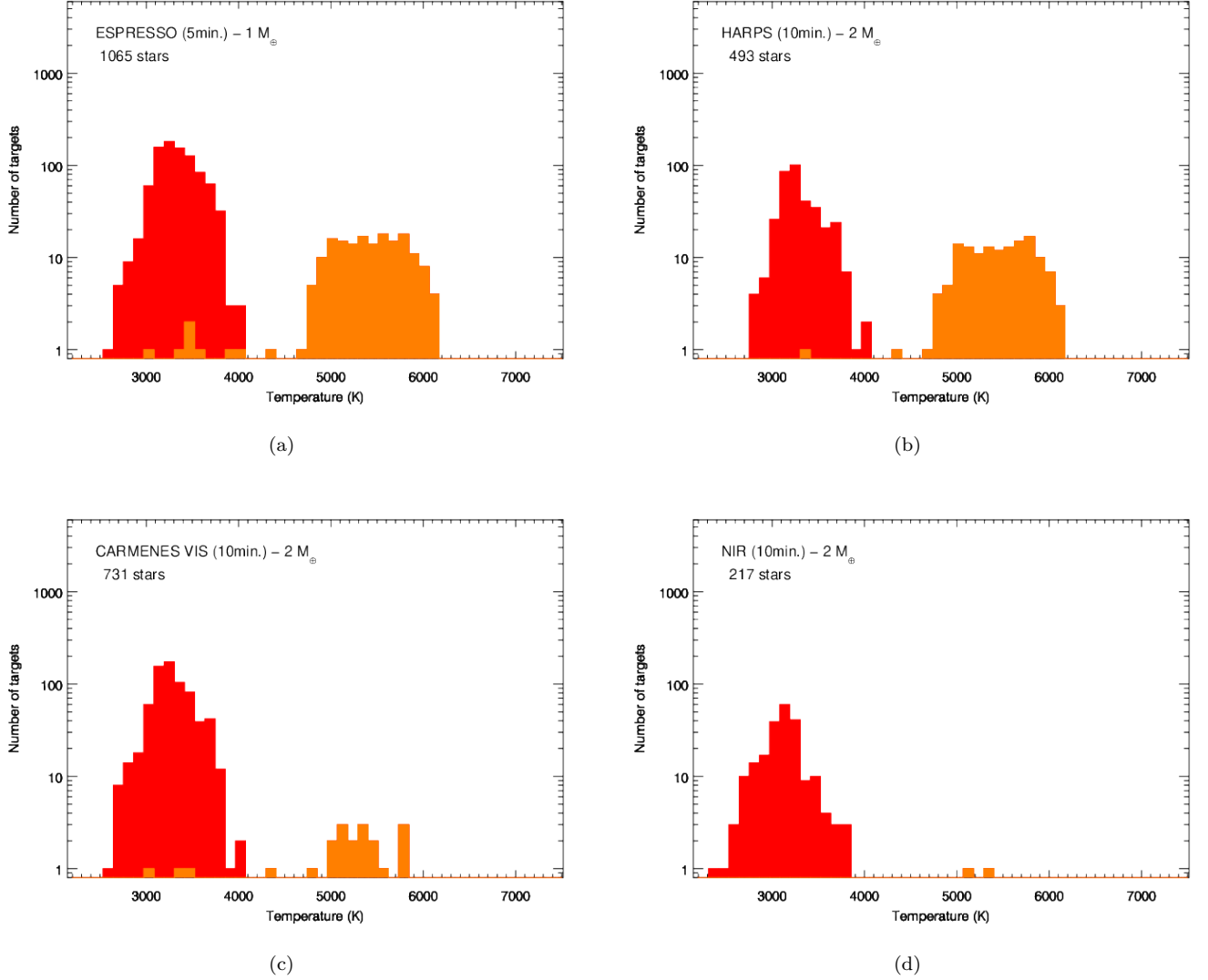


Figure 9. Histogram of stars in which planets of masses less or equal $1 M_{\oplus}$ (ESPRESSO design, upper left panel) and $2 M_{\oplus}$ (all other) can be discovered inside the HZ of the star in a 5 min (ESPRESSO), 10 min (HARPS, CARMENES VIS), and NIR observation. Colors indicate stars from different catalogues as in Fig. 2.

We now focus on the search for planets inside the liquid water habitable zone (HZ) of our sample stars (Kopparapu et al. 2014). For the distance of the HZ to the star, we use the runaway greenhouse limit for $0.1 M_{\oplus}$, which relatively well matches the position of Earth in the solar system (see Fig. 3 of Kopparapu et al. 2014). In Fig. 8, we show for each star the minimum mass of a planet located inside the HZ that causes an RV amplitude, K , as large as the RV photon limit, σ_{RV} , that can be reached within a 10 min exposure (5 min for ESPRESSO), i.e., RV amplitudes identical to the values as shown in Fig. 5. Stars from Gaia DR2 are not shown here because we did not attempt a mass estimate for these stars. We realize that our requirement $K = \sigma_{RV}$ for the determination of a planetary orbit does not capture the full complexity of RV planet discoveries (see, e.g., Garcia-Piquer et al. 2017; Cloutier et al. 2018b,a). Nevertheless, this simple assumption can serve as a useful guideline to characterize the sample of stars suitable for RV work with different instruments.

For the case of ESPRESSO, we see that the RV photon noise potentially allows the detection of planets inside the HZ that are less massive than $1 M_{\oplus}$ around both sun-like stars and M dwarfs. With the 4m-class instruments, we find that RV photon limits can be reached that in principle allow to find planets down to $1 M_{\oplus}$ and below around a small sample of M-dwarfs. For sun-like stars, the HARPS design provides enough information in the brightest targets to see

RV amplitudes caused by planets of a few Earth-masses. The CARMENES VIS and the NIR designs are less efficient in sun-like stars.

In Fig. 9, we show histograms of the stars around which the RV photon noise is as low as the RV amplitude caused by a planet of $M = 2 M_{\oplus}$ inside the star’s HZ if observed with one of the 4m-class instruments, and for a planet of $M = 1 M_{\oplus}$ for the ESPRESSO design. For the latter, we find 1065 stars that fulfill these criteria including both sun-like stars and cooler stars. About half the number of stars (493) but with similar distribution in temperature are available in our sample for HARPS-like instruments (but for a $2 M_{\oplus}$ limit). The distributions of stars for the two redder designs extend down to lower temperatures but contain only very few stars hotter than 4000 K. For the CARMENES VIS design, we find 731 stars in which low-mass planets inside the HZ cause an RV amplitude similar to the RV photon limit. For the NIR design, we find a total number of 217 stars that fulfill our criteria.

6. SUMMARY

To answer the questions (a) what are the minimum detectable masses of planets orbiting the stars in our galactic neighborhood, and (b) with what kind of spectrograph can they be discovered, we construct a sample of well characterized dwarf stars with spectral types F–M from different literature catalogues. This sample contains 46,480 stars and presumably comprises most of the relevant targets for ongoing and planned RV programs. We provide an online-tool where RV photon limits can be calculated for different spectrograph configurations.

Based on empirical information from the HARPS and CARMENES instruments, together with model simulations, we construct a consistent set of values for the RV photon noise achievable in spectroscopic observations at wavelengths between 400 nm and 2400 nm. This information is combined with our knowledge about stellar brightness to estimate the RV photon noise that can be obtained in an observation with a given instrument and telescope. We specifically estimate the RV photon noise for four example configurations: (1) an ESPRESSO-like design at an 8m-class telescope, (2) an optical spectrograph like HARPS at a 4m-telescope, (3) a red optical spectrograph like CARMENES-VIS at a 4m-telescope, and (4) a near-infrared spectrograph covering wavelengths redward of 900 nm at a 4m-telescope (similar to CARMENES-NIR, SPIROU, NIRPS, and GIANO). Comparing instrument performances, we come to the conclusion that an optical design like HARPS (case 2) provides more RV information than a near-IR instrument (case 4) in dwarf stars with temperatures above ~ 3200 K. Compared to the red optical spectrograph (case 3), the optical design (case 2) is more efficient for stellar temperatures above 4000 K.

For our catalogue stars, we determine the RV photon noise after 5 min observations for the ESPRESSO design, and after 10 min observations for the other, and we identify the targets in which this value is lower than 0.1 m s^{-1} for the ESPRESSO design and 1 m s^{-1} for the other. In addition, we determine the minimum mass of planets inside the liquid-water habitable zones that would cause RV amplitudes equal to the RV photon noise for each of the four instrument configurations. For the ESPRESSO design, we find that more than 280 stars provide enough information in a 5-min observation to push the RV photon noise below 0.1 m s^{-1} . These stars include both M dwarfs and sun-like stars. For the 4m-class setups (cases 2–4), we find that the optical, (HARPS) design can reach the RV photon noise limit of 1 m s^{-1} in approx. 10,000 stars. For the red-optical (CARMENES-VIS) design, this number is roughly 3000, and it is about 700 for the NIR design. The optical design is performing best in sun-like stars but there are also hundreds of targets down to temperatures of 3000 K for which this limit is achievable. The red-optical and near-IR designs can reach low photon limits in even cooler stars, but all very-low-mass stars at temperatures below 2700 K are so faint that too few photons for an RV photon limit of 1 m s^{-1} can be collected at any wavelength with a 4m-telescope in 10 min exposures.

As for the number of low-mass planets inside the HZ, we find that those with masses below $1 M_{\oplus}$ can cause an RV amplitude similar to the RV photon noise in more than 1000 stars with the ESPRESSO-like setup using 5 min observations. For the optical setup, we find almost 500 stars in which the RV amplitude caused by a $2 M_{\oplus}$ planet inside the HZ would be larger than the RV photon noise in a 10 min observation. For both instruments, the candidate stars include sun-like and low-mass stars. The red-optical and near-IR setups are optimized for the characterization of low-mass planets around low-mass stars. For the same criteria ($2 M_{\oplus}$ planets and 10 min exposure time), we find more than 700 targets for the red-optical setup, and more than 200 targets for the near-IR instruments. With a few exceptions, these stars are M dwarfs cooler than 4000 K.

Our estimates did not include the effects of instrument stability, individual rotation rates, stellar activity, etc., that are all adding up against the detection of Doppler motion smaller than a few m s^{-1} . Improving instrument strategies, long-term stability, and cross-calibration among different instruments, as well as mitigating the deteriorating effects

of stellar variability are key to the success of RV missions with the goal of finding very-low mass planets. Our analysis shows that current technology can obtain enough spectroscopic information to detect Earth-like planets in a large number of known stars, and our catalogue should help to identify the most suitable targets for current and future RV missions and the search for other Earths.

We are very thankful to R. Cloutier for helpful discussions about radial velocity noise. The RV precision online calculator was developed by Daniel Elkeles. We acknowledge financial support from the DFG Research Unit FOR 2544 “Blue Planets around Red Stars”.

REFERENCES

- Aigrain, S., Pont, F., & Zucker, S. 2012, *MNRAS*, 419, 3147, doi: [10.1111/j.1365-2966.2011.19960.x](https://doi.org/10.1111/j.1365-2966.2011.19960.x)
- Andrae, R., Fouesneau, M., Creevey, O., et al. 2018, ArXiv e-prints. <https://arxiv.org/abs/1804.09374>
- Anglada-Escudé, G., Tuomi, M., Gerlach, E., et al. 2013, *A&A*, 556, A126, doi: [10.1051/0004-6361/201321331](https://doi.org/10.1051/0004-6361/201321331)
- Anglada-Escudé, G., Arriagada, P., Tuomi, M., et al. 2014, *MNRAS*, 443, L89, doi: [10.1093/mnras/llu076](https://doi.org/10.1093/mnras/llu076)
- Anglada-Escudé, G., Amado, P. J., Barnes, J., et al. 2016, *Nature*, 536, 437, doi: [10.1038/nature19106](https://doi.org/10.1038/nature19106)
- Artigau, É., Malo, L., Doyon, R., et al. 2018, *AJ*, 155, 198, doi: [10.3847/1538-3881/aab77d](https://doi.org/10.3847/1538-3881/aab77d)
- Astudillo-Defru, N., Delfosse, X., Bonfils, X., et al. 2017, *A&A*, 600, A13, doi: [10.1051/0004-6361/201527078](https://doi.org/10.1051/0004-6361/201527078)
- Baraffe, I., Chabrier, G., Allard, F., & Hauschildt, P. H. 1998, *A&A*, 337, 403
- Beatty, T. G., & Gaudi, B. S. 2015, *PASP*, 127, 1240, doi: [10.1086/684264](https://doi.org/10.1086/684264)
- Bonfils, X., Delfosse, X., Udry, S., et al. 2013, *A&A*, 549, A109, doi: [10.1051/0004-6361/201014704](https://doi.org/10.1051/0004-6361/201014704)
- Bottom, M., Muirhead, P. S., Johnson, J. A., & Blake, C. H. 2013, *PASP*, 125, 240, doi: [10.1086/670174](https://doi.org/10.1086/670174)
- Bouchy, F., Pepe, F., & Queloz, D. 2001, *A&A*, 374, 733, doi: [10.1051/0004-6361:20010730](https://doi.org/10.1051/0004-6361:20010730)
- Brewer, J. M., Fischer, D. A., Valenti, J. A., & Piskunov, N. 2016, *ApJS*, 225, 32, doi: [10.3847/0067-0049/225/2/32](https://doi.org/10.3847/0067-0049/225/2/32)
- Butler, R. P., Marcy, G. W., Williams, E., et al. 1996, *PASP*, 108, 500, doi: [10.1086/133755](https://doi.org/10.1086/133755)
- Cegla, H. M., Stassun, K. G., Watson, C. A., Bastien, F. A., & Pepper, J. 2014, *ApJ*, 780, 104, doi: [10.1088/0004-637X/780/1/104](https://doi.org/10.1088/0004-637X/780/1/104)
- Chandler, C. O., McDonald, I., & Kane, S. R. 2016, *AJ*, 151, 59, doi: [10.3847/0004-6256/151/3/59](https://doi.org/10.3847/0004-6256/151/3/59)
- Chaplin, W. J., Cegla, H. M., Watson, C. A., Davies, G. R., & Ball, W. H. 2019, *AJ*, 157, 163, doi: [10.3847/1538-3881/ab0c01](https://doi.org/10.3847/1538-3881/ab0c01)
- Cloutier, R., Doyon, R., Bouchy, F., & Hébrard, G. 2018a, *AJ*, 156, 82, doi: [10.3847/1538-3881/aacea9](https://doi.org/10.3847/1538-3881/aacea9)
- Cloutier, R., Artigau, É., Delfosse, X., et al. 2018b, *AJ*, 155, 93, doi: [10.3847/1538-3881/aaa54e](https://doi.org/10.3847/1538-3881/aaa54e)
- Collier Cameron, A., Mortier, A., Phillips, D., et al. 2019, *MNRAS*, 487, 1082, doi: [10.1093/mnras/stz1215](https://doi.org/10.1093/mnras/stz1215)
- Connes, P. 1985, *Ap&SS*, 110, 211, doi: [10.1007/BF00653671](https://doi.org/10.1007/BF00653671)
- Demory, B.-O., Ségransan, D., Forveille, T., et al. 2009, *A&A*, 505, 205, doi: [10.1051/0004-6361/200911976](https://doi.org/10.1051/0004-6361/200911976)
- Donati, J.-F., Kouach, D., Lacombe, M., et al. 2017, *SPIRou: A nIR Spectropolarimeter/High-precision Velocimeter for the CFHT*, 107
- Dumusque, X. 2018, *A&A*, 620, A47, doi: [10.1051/0004-6361/201833795](https://doi.org/10.1051/0004-6361/201833795)
- Figueira, P., Adibekyan, V. Z., Oshagh, M., et al. 2016, *A&A*, 586, A101, doi: [10.1051/0004-6361/201526900](https://doi.org/10.1051/0004-6361/201526900)
- Fischer, D. A., Anglada-Escudé, G., Arriagada, P., et al. 2016, *PASP*, 128, 066001, doi: [10.1088/1538-3873/128/964/066001](https://doi.org/10.1088/1538-3873/128/964/066001)
- Fouqué, P., Moutou, C., Malo, L., et al. 2018, *MNRAS*, 475, 1960, doi: [10.1093/mnras/stx3246](https://doi.org/10.1093/mnras/stx3246)
- Gaia Collaboration, Brown, A. G. A., Vallenari, A., et al. 2018, ArXiv e-prints. <https://arxiv.org/abs/1804.09365>
- Gaia Collaboration, Prusti, T., de Bruijne, J. H. J., et al. 2016, *A&A*, 595, A1, doi: [10.1051/0004-6361/201629272](https://doi.org/10.1051/0004-6361/201629272)
- Gaidos, E., Mann, A. W., Lépine, S., et al. 2014, *MNRAS*, 443, 2561, doi: [10.1093/mnras/stu1313](https://doi.org/10.1093/mnras/stu1313)
- Garcia-Piquer, A., Morales, J. C., Ribas, I., et al. 2017, *A&A*, 604, A87, doi: [10.1051/0004-6361/201628577](https://doi.org/10.1051/0004-6361/201628577)
- Golimowski, D. A., Leggett, S. K., Marley, M. S., et al. 2004, *AJ*, 127, 3516, doi: [10.1086/420709](https://doi.org/10.1086/420709)
- Haywood, R. D., Collier Cameron, A., Unruh, Y. C., et al. 2016, *MNRAS*, 457, 3637, doi: [10.1093/mnras/stw187](https://doi.org/10.1093/mnras/stw187)
- Henry, T. J., Jao, W.-C., Subasavage, J. P., et al. 2006, *AJ*, 132, 2360, doi: [10.1086/508233](https://doi.org/10.1086/508233)
- Henry, T. J., Jao, W.-C., Winters, J. G., et al. 2016, in *American Astronomical Society Meeting Abstracts*, Vol. 227, American Astronomical Society Meeting Abstracts, 142.01

- Hojjatpanah, S., Figueira, P., Santos, N. C., et al. 2019, arXiv e-prints, arXiv:1908.04627.
<https://arxiv.org/abs/1908.04627>
- Huélamo, N., Figueira, P., Bonfils, X., et al. 2008, *A&A*, 489, L9, doi: [10.1051/0004-6361/200810596](https://doi.org/10.1051/0004-6361/200810596)
- Husser, T.-O., Wende-von Berg, S., Dreizler, S., et al. 2013, *A&A*, 553, A6, doi: [10.1051/0004-6361/201219058](https://doi.org/10.1051/0004-6361/201219058)
- Jeffers, S. V., Schöfer, P., Lamert, A., et al. 2018, *A&A*, 614, A76, doi: [10.1051/0004-6361/201629599](https://doi.org/10.1051/0004-6361/201629599)
- Kenyon, S. J., & Hartmann, L. 1995, *ApJS*, 101, 117, doi: [10.1086/192235](https://doi.org/10.1086/192235)
- Kopparapu, R. K., Ramirez, R. M., SchottelKotte, J., et al. 2014, *ApJL*, 787, L29, doi: [10.1088/2041-8205/787/2/L29](https://doi.org/10.1088/2041-8205/787/2/L29)
- Marconi, A., Di Marcantonio, P., D’Odorico, V., et al. 2016, in *Proc. SPIE*, Vol. 9908, Ground-based and Airborne Instrumentation for Astronomy VI, 990823
- Martín, E. L., Guenther, E., Zapatero Osorio, M. R., Bouy, H., & Wainscoat, R. 2006, *ApJL*, 644, L75, doi: [10.1086/505343](https://doi.org/10.1086/505343)
- Mayor, M., Pepe, F., Queloz, D., et al. 2003, *The Messenger*, 114, 20
- Mayor, M., Bonfils, X., Forveille, T., et al. 2009, *A&A*, 507, 487, doi: [10.1051/0004-6361/200912172](https://doi.org/10.1051/0004-6361/200912172)
- Mohanty, S., & Basri, G. 2003, *ApJ*, 583, 451, doi: [10.1086/345097](https://doi.org/10.1086/345097)
- Newton, E. R., Irwin, J., Charbonneau, D., et al. 2017, *ApJ*, 834, 85, doi: [10.3847/1538-4357/834/1/85](https://doi.org/10.3847/1538-4357/834/1/85)
- Nordström, B., Mayor, M., Andersen, J., et al. 2004, *A&A*, 418, 989, doi: [10.1051/0004-6361:20035959](https://doi.org/10.1051/0004-6361:20035959)
- Origlia, L., Oliva, E., Baffa, C., et al. 2014, in *Proc. SPIE*, Vol. 9147, Ground-based and Airborne Instrumentation for Astronomy V, 91471E
- Passegger, V. M., Reiners, A., Jeffers, S. V., et al. 2018, *A&A*, 615, A6, doi: [10.1051/0004-6361/201732312](https://doi.org/10.1051/0004-6361/201732312)
- Pepe, F., Molaro, P., Cristiani, S., et al. 2014, *Astronomische Nachrichten*, 335, 8, doi: [12.1002/asna.201312004](https://doi.org/12.1002/asna.201312004)
- Perryman, M. 2014, *The Exoplanet Handbook*
- Plavchan, P., Latham, D., Gaudi, S., et al. 2015, *ArXiv e-prints*. <https://arxiv.org/abs/1503.01770>
- Quirrenbach, A., Amado, P. J., Caballero, J. A., et al. 2016, in *Proc. SPIE*, Vol. 9908, Ground-based and Airborne Instrumentation for Astronomy VI, 990812
- Rauer, H., Catala, C., Aerts, C., et al. 2014, *Experimental Astronomy*, 38, 249, doi: [10.1007/s10686-014-9383-4](https://doi.org/10.1007/s10686-014-9383-4)
- Reiners, A., & Basri, G. 2009, *ApJ*, 705, 1416, doi: [10.1088/0004-637X/705/2/1416](https://doi.org/10.1088/0004-637X/705/2/1416)
- Reiners, A., Bean, J. L., Huber, K. F., et al. 2010, *ApJ*, 710, 432, doi: [10.1088/0004-637X/710/1/432](https://doi.org/10.1088/0004-637X/710/1/432)
- Reiners, A., Joshi, N., & Goldman, B. 2012, *AJ*, 143, 93, doi: [10.1088/0004-6256/143/4/93](https://doi.org/10.1088/0004-6256/143/4/93)
- Reiners, A., Shulyak, D., Anglada-Escudé, G., et al. 2013, *A&A*, 552, A103, doi: [10.1051/0004-6361/201220437](https://doi.org/10.1051/0004-6361/201220437)
- Reiners, A., Zechmeister, M., Caballero, J. A., et al. 2018, *A&A*, 612, A49, doi: [10.1051/0004-6361/201732054](https://doi.org/10.1051/0004-6361/201732054)
- Reinhold, T., Reiners, A., & Basri, G. 2013, *A&A*, 560, A4, doi: [10.1051/0004-6361/201321970](https://doi.org/10.1051/0004-6361/201321970)
- Ricker, G. R., Winn, J. N., Vanderspek, R., et al. 2015, *Journal of Astronomical Telescopes, Instruments, and Systems*, 1, 014003, doi: [10.1117/1.JATIS.1.1.014003](https://doi.org/10.1117/1.JATIS.1.1.014003)
- Rodler, F., Del Burgo, C., Witte, S., et al. 2011, *A&A*, 532, A31, doi: [10.1051/0004-6361/201015490](https://doi.org/10.1051/0004-6361/201015490)
- Santos, N. C., Mayor, M., Naef, D., et al. 2000, *A&A*, 361, 265
- Scalo, J., Kaltenegger, L., Segura, A. G., et al. 2007, *Astrobiology*, 7, 85, doi: [10.1089/ast.2006.0125](https://doi.org/10.1089/ast.2006.0125)
- Szentgyorgyi, A., Baldwin, D., Barnes, S., et al. 2016, in *Proc. SPIE*, Vol. 9908, Ground-based and Airborne Instrumentation for Astronomy VI, 990822
- Tarter, J. C., Backus, P. R., Mancinelli, R. L., et al. 2007, *Astrobiology*, 7, 30, doi: [10.1089/ast.2006.0124](https://doi.org/10.1089/ast.2006.0124)
- Terrien, R. C., Mahadevan, S., Deshpande, R., & Bender, C. F. 2015, *ApJS*, 220, 16, doi: [10.1088/0067-0049/220/1/16](https://doi.org/10.1088/0067-0049/220/1/16)
- Tronsgaard, R., Buchhave, L. A., Wright, J. T., Eastman, J. D., & Blackman, R. T. 2019, *MNRAS*, 489, 2395, doi: [10.1093/mnras/stz2181](https://doi.org/10.1093/mnras/stz2181)
- Wildi, F., Blind, N., Reshetov, V., et al. 2017, in *Society of Photo-Optical Instrumentation Engineers (SPIE) Conference Series*, Vol. 10400, Society of Photo-Optical Instrumentation Engineers (SPIE) Conference Series, 1040018
- Wright, J. T. 2005, *PASP*, 117, 657, doi: [10.1086/430369](https://doi.org/10.1086/430369)
- Wright, J. T., & Robertson, P. 2017, *Research Notes of the American Astronomical Society*, 1, 51, doi: [10.3847/2515-5172/aaa12e](https://doi.org/10.3847/2515-5172/aaa12e)
- Zechmeister, M., Reiners, A., Amado, P. J., et al. 2018, *A&A*, 609, A12, doi: [10.1051/0004-6361/201731483](https://doi.org/10.1051/0004-6361/201731483)

APPENDIX

A. STAR TABLE

Table 5. Catalogue of F–M stars. Targets are taken from the catalogues listed in Table 1. RV limits and HZ-detection limits are for 5 min in the case of the ESPRESSO design (ES), 10 min for HARPS (HA) and CARMENES VIS (CV), and 20 min for the NIR instrument. See Table 4 for a detailed description of the instrument configurations.

ID	T_{eff} (K)	d (pc)	Mass (M_{\odot})	V (mag)	J (mag)	L (L_{\odot})	HZD (AU)	Ref	RV limit (m s^{-1})			HZ-detection limit (M_{\oplus})				
									ES	HA	CV	NIR	ES	HA	CV	NIR
2MASS J14294291-6240465	2883	1.3	0.14	10.76	5.36	0.003	0.06	Gai	0.12	0.41	0.23	0.32	0.13	0.42	0.24	0.33
2MASS J17574849+0441405	3237	1.8	0.14	9.49	5.24	0.003	0.06	Gai	0.08	0.26	0.19	0.46	0.09	0.27	0.20	0.47
2MASS J10562886+0700527	2865	2.4	0.14	12.94	7.09	0.003	0.06	Gai	0.32	1.14	0.56	0.72	0.33	1.17	0.58	0.74
2MASS J11032023+3558117	3593	2.5	0.46	7.51	4.20	0.028	0.18	Gai	0.05	0.17	0.13	0.31	0.17	0.54	0.42	1.00
2MASS J18494929-2350101	3213	3.0	0.14	10.41	6.22	0.003	0.06	Gai	0.14	0.44	0.31	0.73	0.14	0.45	0.32	0.75
2MASS J23415498+4410407	3005	3.2	0.14	12.41	6.88	0.003	0.06	Gai	0.23	0.79	0.46	0.75	0.24	0.82	0.48	0.77
HD 22049	5116	3.2	0.82	3.72		0.388	0.65	Nor	0.03	0.05	0.11	0.19	0.21	0.44	0.92	1.55
2MASS J11474440+0048164	3145	3.4	0.14	11.21	6.51	0.003	0.06	Gai	0.17	0.54	0.37	0.76	0.17	0.56	0.38	0.78
HD 61421	6683	3.5	1.53	0.37		3.934	1.89	Nor	0.08	0.16	0.43	0.44	1.50	3.11	8.11	8.41
2MASS J18424688+5937374	3334	3.5	0.25	10.00	5.72	0.009	0.10	Gai	0.10	0.33	0.25	0.58	0.19	0.60	0.45	1.04
2MASS J00182256+4401222	3669	3.6	0.50	8.15	5.25	0.036	0.21	Gai	0.09	0.29	0.23	0.53	0.32	1.03	0.82	1.91
2MASS J00182549+4401376	3282	3.6	0.19	11.08	6.79	0.006	0.09	Gai	0.18	0.58	0.42	0.96	0.25	0.83	0.59	1.36
2MASS J08294949+2646348	2809	3.6	0.14	14.16	8.23	0.003	0.06	Gai	0.69	2.72	1.09	1.24	0.71	2.80	1.12	1.28
2MASS J18424666+5937499	3392	3.6	0.30	8.92	5.19	0.013	0.13	Gai	0.08	0.25	0.19	0.45	0.17	0.55	0.42	0.98
HD 10700	5345	3.6	0.81	3.50		0.451	0.69	Nor	0.03	0.05	0.12	0.20	0.22	0.46	0.97	1.64
2MASS J01123052-1659570	3062	3.7	0.14	11.96	7.26	0.003	0.06	Gai	0.27	0.92	0.55	0.97	0.27	0.94	0.56	1.00
2MASS J03355969-4430453	2999	3.7	0.14	13.06	7.52	0.003	0.06	Gai	0.33	1.17	0.64	1.01	0.34	1.20	0.66	1.04
2MASS J07272450+0513329	3317	3.8	0.23	9.81	5.71	0.008	0.10	Gai	0.10	0.33	0.25	0.57	0.17	0.55	0.41	0.96
2MASS J02530084+1652532	2700	3.9	0.14	14.51	8.39	0.003	0.06	Gai	1.06	4.67	1.59	1.25	1.09	4.81	1.64	1.28
2MASS J05114046-4501051	3695	3.9	0.52	8.93	5.82	0.039	0.22	Gai	0.12	0.39	0.30	0.71	0.44	1.45	1.14	2.66
2MASS J21171534-3852022	3776	3.9	0.56	6.75	4.05	0.048	0.24	Gai	0.05	0.16	0.14	0.31	0.22	0.66	0.57	1.27